IAC-18,D1,3,3,x47544

A HIGHLY INTEGRATED NAVIGATION UNIT FOR ON-ORBIT SERVICING MISSIONS

Vincenzo Capuano [(1)], Roberto Opromolla[(4)], Giovanni Cuciniello [(2)], Vincenzo Pesce [(3)], Salvatore Sarno[(4)], Giuseppe Capuano [(1)], Michelle Lavagna [(3)], Michele Grassi[(4)], Federico Corraro [(2)], Paolo Tabacco[(5)], Marco Adinolfi [(1)], Maria Libera Battagliere [(6)], Alberto Tuozzi[(6)]

[(1)] *Techno System Dev. S.r.l., Via Provinciale Pianura 2, San Martino Zona Industriale, 80078 Pozzuoli Italy, vcapuano@tsd-space.it, gcapuano@tsd-space.it*
[(2)]*Centro italiano ricerche aerospaziali (CIRA s.c.p.a.), Via Maiorise 1, 81043 Capua CE, Italy, g.cuciniello@cira.it, f.corraro@cira.it*
[(3)]*Politecnico di Milano, Aerospace Science and Technology Department, via La Masa, 34, 20156 Milano, Italy, vincenzo.pesce@polimi.it, michelle.lavagna@polimi.it*
[(4)]*University of Naples "Federico II", Dept. of Industrial Engineering, P.le Tecchio 80, 80125, Napoli, Italy, roberto.opromolla@unina.it, salvatore.sarno@unicampania.it, michele.grassi@unina.it*
[(5)]*Space Technology S.r.l., Via dell'Orsa Maggiore, 21, 00144 Roma, Italy, tabacco@spacetechnology.it, meta@ spacetechnology.it*
[(6)]*Agenzia Spaziale Italiana (ASI), Via del Politecnico snc, 00133 Roma, Italy, maria.battagliere@asi.it*

ABSTRACT

VINAG (VISION/INS integrated Navigation Assisted by GNSS) is a highly integrated multisensor navigation unit, particularly conceived for On-Orbit Servicing missions. The system is designed to provide all-in-one, on-board real time autonomous absolute navigation as well as pose determination of an uncooperative known object orbiting in LEO (Low Earth Orbit), GEO (GEosynchronous Orbits) and possibly in HEO (Highly Earth Orbit). The system VINAG is under development by a team of Italian companies and universities, co-financed by the Italian Space Agency. Thanks to a tight optimized integration of its subsystems, VINAG is characterized by a low power and mass total budgets and therefore it is suitable for small and very small satellites.

In order to provide both 1) absolute orbit and attitude determination and 2) vision-based pose determination, the unit integrates three metrology systems: a Cameras Subsystem (a monocular camera and a Star sensor), an Inertial Measurement Unit (IMU) and a GNSS (Global Navigation Satellite System) receiver.

In this paper, we briefly introduce the complete system architecture, the adopted algorithms and then we detail the adopted hardware design solutions. In addition, we describe preliminary numerical simulation results obtained for different orbits from LEO to GEO carried out for the validation phase of VINAG.

1. INTRODUCTION

In space applications that rely on autonomy, precision, robustness, adaptability to different scenarios, as missions of On-Orbit Servicing (OOS), debris removal, or Formation Flying (FF), a tight integration of different navigation technologies that sums their advantages and compensates their limitations, can play a key role, having certainly many advantages. It can provide more accurate and more robust navigation than using the single technology individually. Moreover, it is possible to avoid non-efficient replication of hardware (HW) components and basic functionalities, as computing, power supply, data interface, etc., with a resultant saving in mass, volume and power consumption.

VINAG (VISION/INS integrated Navigation Assisted by GNSS) is a highly integrated multisensor navigation unit, specifically designed for On-Orbit Servicing missions. The system is conceived to provide all-in-one, on-board real time autonomous absolute navigation as well as pose determination of an uncooperative known object orbiting in LEO (Low Earth Orbit), GEO (GEosynchronous Orbits) and possibly in HEO (Highly Earth Orbit). The system VINAG is currently under development by a team of Italian companies and universities, co-financed by the Italian Space Agency. Thanks to a smart and tight integration of its subsystems, VINAG is characterized by a low power and mass total budgets and therefore it is suitable for small and very small satellites.

In order to provide both 1) absolute orbit and attitude determination and 2) vision-based pose determination, the unit integrates three metrology systems: a Cameras Subsystem (a monocular camera and a Star sensor), an Inertial Measurement Unit (IMU) and a GNSS (Global Navigation Satellite System) receiver.

The VINAG HW includes the VINAG Central Unit (VCU), the Inertial Measurement Unit (IMU) Module and VINAG Cameras System. The latter comprehends two redundant CMOS monocular cameras and a Star sensor, while the VCU includes the Visual navigation & Data Fusion Module (VDFM), a GNSS Receiver Module and the Power Conditioning & Distribution Module (PCDM). The monocular camera of TSD Space S.r.l. and the GNSS receiver of Space Technology S.r.l have been specifically

customized for the VINAG system, while the VDFM and the PCDM completely designed fit-for-purpose by TSD Space S.r.l., prime of the project.

The architecture, some of the navigation algorithms and preliminary simulation results of the performance of VINAG, were already described in our previous work [1], which also provides a more extensive introduction, including a comparison with other existing similar systems. This paper is essentially a follow up on the development progress.

In Section 2, we briefly introduce the complete system architecture, while in Section 3 the adopted algorithms. In Section 4, we detail the adopted hardware design solutions. Section 5 outlines the SW and HW portioning of the navigation algorithms. In Section 6, we describe the numerical simulation results obtained in LEO and GEO, carried out for the validation phase of VINAG.

2. SYSTEM ARCHITECTURE

Figure 1 illustrates high level functional architecture of VINAG. For absolute orbit and attitude determination, a nonlinear Kalman filter is used to fuse GNSS and Star sensor observations with inertial measurements and with a model of the absolute translational and rotational dynamics. In relative navigation, images of the orbiting target are acquired by a monocular CMOS camera to estimate its relative pose (position and attitude). This first estimate is further refined, with a translational dynamics filter and a rotational kinematics filter.

The following sections, separately, provide a more detailed description of the approaches and algorithms for absolute and relative navigation.
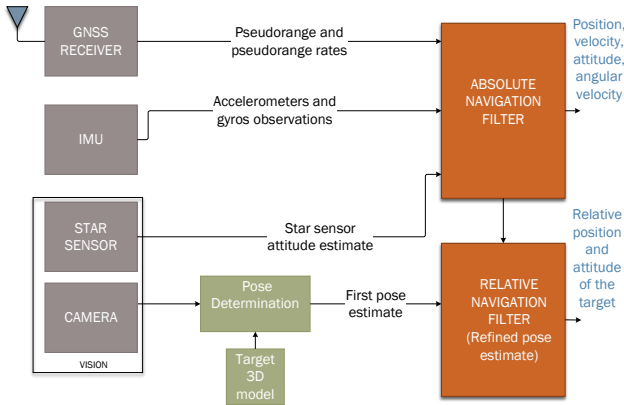

Figure 1. Functional architecture of VINAG.

3. NAVIGATION ALGORITHMS

3.1 Absolute Navigation

The integration of GNSS, IMU and Star sensor observations enables orbit and attitude determination.

The Absolute Navigation algorithm consists in a single (centralized) Square-Root Unscented Kalman Filter [2]

running at the maximum available measurement rate (100Hz). The following set of constraints was assumed to feed the trade-off and design phases:

- Available sensors: Star Tracker that provides the unbiased (and noisy) attitude measurement with an update rate of 5Hz, an Inertial Measurement Unit (IMU) that provides both biased accelerometer and angular velocity measurement at 100Hz, a Global Navigation Satellite System (GNSS) multi-constellation, single-frequency receiver with 30 channels and an update rate of 1Hz.
- The available sensors are assumed already compensated for systematic source of errors (i.e. mutual and installation misalignment, temperature variations cross-coupling, non-linearity, relativistic effects and so on) already compensated or negligible.
- The gravitational model used in the absolute navigation filter equations assumes a homogenous spherical Earth as described in [3]:

$$a_g = -\frac{GM}{|p|^3}\begin{bmatrix} x - \frac{3x}{2}J_2\left(\frac{R_e}{|p|}\right)^2\left(5\frac{z^2}{|p|^2}-1\right) \\ y - \frac{3y}{2}J_2\left(\frac{R_e}{|p|}\right)^2\left(5\frac{z^2}{|p|^2}-1\right) \\ z - \frac{3z}{2}J_2\left(\frac{R_e}{|p|}\right)^2\left(5\frac{z^2}{|p|^2}-3\right) \end{bmatrix} \quad (1)$$

Where a_g is the gravitational acceleration, GM is the product of the universal gravity constant and the Earth mass (that in the WGS84 system is equal to 3.9860050e14 m^3/s^2), R_e is the equatorial Earth radius (6378137 m) and J_2 is the 2nd degree harmonic coefficient.

- Moreover, in case of unpowered flight, the non-gravitational perturbations are essentially due to the atmospheric drag (especially for low orbits), which rapidly decreases for higher orbits, albedo, and Solar pressure that becomes the uppermost for GEO and higher orbits [4].

The standard UKF is a nonlinear filtering technique based on the concept of Unscented Transformation (UT), a formal mathematical method for propagating a probability distribution through a nonlinear transformation. The UKF provides at least second-order accurate evaluations of the first two statistical moments of the unknowns, enabling a complete and structured statistical characterization of the estimated variables and leading to a reliable evaluation of the uncertainties on the estimations. Nevertheless, like all Kalman filters, the UKF performs the estimation in two sequential phases. Firstly, a dynamic model, provides a time propagation of the estimation (prediction phase). Then, at each time step, the available measurements are used to refine the estimation (correction phase). Furthermore, a specific formulation called Square-Root

UKF allows to mitigate the effects of numerical instability, positive semi-definitiveness of the state covariance and so on.

The orbital filer model is based on an Earth Centred Inertial (ECI) reference frame integration model. A classical Cartesian formulation of the motion equations and attitude kinematics is assumed:

$$\dot{p} = v \tag{2}$$

$$\dot{v} = a_{ng} + a_g \tag{3}$$

$$\dot{q} = \frac{1}{2}\Omega(\omega) \tag{4}$$

Where $p = [x, y, z]^T$ and v are respectively the position and velocity of the VINAG system in the ECI reference frame and q is the quaternion representing the VINAG system attitude with respect to the ECI frame. $\Omega(\omega)$ is the skew matrix function of the angular velocity $\omega = [\omega_x, \omega_y, \omega_z]^T$. The acceleration a_{ng} represents the total non-gravitational acceleration, while a_g is the gravitational acceleration defined in (1).

In addition, different Gauss-Markov processes model the non-gravitational acceleration, the gyro bias ω_b, the GNSS receiver time delay δt and related drift k_t as reported below:

$$\dot{a_{ng}} = \eta_{ng} \tag{5}$$

$$\dot{\omega_b} = \eta_\omega \tag{6}$$

$$\dot{\delta t} = k_t + \eta_{\delta t} \tag{7}$$

$$\dot{k_t} = \eta_{k_t} \tag{8}$$

where ω_b is the gyro bias, while $\eta_{ng}, \eta_\omega, \eta_{\delta t}$ and η_{k_t} are the respective zero mean white Gaussian noise processes related to the non-gravitational accelerations a_{ng}, the gyro bias, GPS receiver timer bias δt and drift k_t.

The total number of the process states is 18, but using a minimal attitude representation based on the Rodrigues Parameters [5], allows reducing the total internal filter state dimension to 17.

In order to perform the model propagation phase, the dynamic model equations are properly discretized using a 1th and/or 2nd order Taylor series approximation, including while equation (4) as described in [6].

With reference to an UKF approach, while state elements other than quaternions (or Rodrigues parameters) are defined in a Cartesian space allowing normal algebraic manipulation, the quaternion statistical propagation could yield to a non-unity quaternion estimation [5]. In order to guarantee a unity quaternion propagation/correction a specific algorithm proposed in [7] was adopted allowing averaging on a unit hypersphere manifold.

The measurements of the orbital filter in this study include: i) up to 30 pseudoranges and 30 pseudorange rate measurements from GNSS receiver related to the current visible satellites, ii) attitude measurements from Star sensor, iii) angular velocity measurements from the gyroscopes, iv) acceleration measurements from accelerometers (used only during powered flight).

Finally, a dedicated masking algorithm was implemented in case of GEO (or higher) orbits. Specifically, low elevation satellites' measurements were discarded in order to avoid strongly auto-correlated error measurement due to relevant atmospheric delays [8].

3.2 Relative Navigation
The relative navigation is performed employing a loosely-coupled architecture. In fact, two separate, consecutive blocks constitute the navigation algorithm. First, the pose determination block provides an estimate of the relative target/chaser pose (position and orientation) by analyzing the acquired images. Then, the result of this process is fed to the navigation filter block. A loosely-coupled architecture for relative navigation is preferred over a tightly-coupled architecture (processing image features directly within a filtering scheme) because, for the scenarios of interest to this work, i.e., On Orbit Servicing (OOS) and Active Debris Removal (ADR), the uncooperative target is usually known. If the basic information about the target geometry is available, loosely-coupled architectures are typically preferred. In fact, this additional information can be directly exploited during the vision-based pose estimation step.

Another important feature concerns the incorporation of the absolute state estimate of the chaser spacecraft in the filtering process. In fact, a precise determination of the chaser true anomaly, that is used to propagate the relative translational dynamics equations in the filter prediction step, is needed. In literature, similar works [9] neglect the possible noise associated to this quantity. However, a noisy fluctuation of the chaser true anomaly can strongly affect the filter robustness and stability. In this work, this explicit dependence is considered and analyzed.

Relative navigation filter
In this work, we propose a decoupled architecture for the relative navigation filter. In fact, considering a rigid spacecraft without external disturbances, the translational and rotational dynamics can be completely decoupled. In this way, robust linear strategies can be employed for the translational part and advanced filtering techniques can be adopted for the rotational part. A decoupled architecture has the disadvantage of neglecting all the coupling effects present in real applications. However, in the considered scenarios of this work, the nature of the problem and the classical limited operations duration suggest decoupling the relative translational and rotational dynamics. Another

advantage of such architecture is that, typically, the determination of the relative position is usually more robust with respect to relative attitude estimation, which is more prone to errors and ambiguities. For this reason, a decoupled strategy guarantees a more robust control of the proximity phase even with poor relative attitude estimation. The proposed architecture consists of a linear H-∞ Filter for the translational motion and a 2nd Order Non-linear Filter on the Special Orthogonal group (SO(3)) for the rotational part.

Translational filter

The translational filter is implemented as an H-∞ Filter. The standard Kalman filter is the optimal estimator for linear systems with zero-mean Gaussian process and measurement noise. However, a robust approach is preferred when these assumptions are not satisfied. A classical robust filter is the H-∞ filter or also minimax filter. It minimizes the ∞-norm of the estimation error without making any restrictive assumptions about the statistics of the process and measurement noise [10]. As explained before, the measurements are the output of the pose estimation block. The formulation of the H-∞ Filter constraint the choice to linear relative dynamics model. In this work, the authors used the formulation by Yamanaka and Ankersen [11] as filter dynamical model, a linearized formulation for arbitrary elliptical orbits.

Rotational filter

For the rotation part, a second-order minimum energy filter on the Lie group is implemented. Recently, minimum energy filters on SO(3) are shown to outperform the classical Multiplicative Extended Kalman Filter [12]. In this paper, a modification to the second-order minimum energy filter proposed by Saccon [13] is introduced without considering the dynamics of the system. This particular formulation of the filter can be adopted also in the case of poor knowledge of the inertia properties of the target spacecraft. For the detailed derivation of the filter, please see [1].

Monocular pose determination

The pose determination block, designed for the relative navigation architecture presented in the previous sub-section, is based on a monocular camera system. Consequently, it includes all the processing functions needed to determine a set of parameters describing the relative position and attitude of the observed target with respect to the camera, starting from raw 2D images. Specifically, the attitude of the Camera Reference Frame (CRF) with respect to the Target body Reference Frame (TRF) is represented by a rotation matrix (R_{TC}), while the relative position of the target with respect to the camera is given by a position vector (t) which is directed from CRF to TRF and is expressed in CRF. In the most general case, the pose parameters are representative of the relative position and attitude between the body reference frames of

the chaser and target. However, the attitude and position of the camera in the chaser body frame is given by the so-called mounting parameters which are fixed and can be determined by means of an off-line calibration procedure (i.e., before mission start).

Pose determination includes two main processing steps, i.e. acquisition and tracking. The acquisition is carried out when the pose parameters are completely unknown. Thus, its output is an input of the overall filtering architecture. Instead, tracking is performed when a pose estimate corresponding to a previous time instant is available. This pose solution is used to initialize the tracking algorithm and it can be provided by either the acquisition tool, or the navigation filter (if the tracking process has already started).

Both the acquisition and tracking functions are entrusted to model-based algorithms, which allow determining the pose parameters by matching data extracted from the acquired images with a target model typically built off-line [14]. The choice of using model-based techniques is compliant to the typology of mission scenarios for which VINAG is conceived. Indeed, most of the related targets are known objects (though uncooperative, i.e., not equipped either with a communication link or with ad-hoc active/passive artificial markers). Specifically, feature-based approaches are presented in this work, which aim at finding the set of parameters providing the best estimate of the optimal match between natural features (e.g. corner or edges) extracted from the acquired images and the target model. These model-based approaches require three online steps, as shown in Figure 2. First, the raw camera output, i.e., an intensity (grey-level) image, is processed to extract a set of 2D features. Second, correspondences must be determined among the features and the target model. Finally, the pose parameters can be estimated by solving the Perspective-*n*-Points (P*n*P) problem [15].
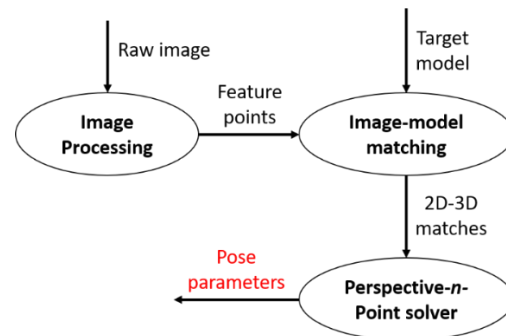

Figure 2. General architecture of the feature-based algorithms proposed for pose acquisition and tracking. The processing steps are highlighted using the bold type. The final output is highlighted using the bold red type.

Before entering the details about the algorithmic solutions adopted in VINAG for each processing step for pose estimation identified in Fig. X, it is important to outline that while existing techniques can be applied to solve the

PnP problem [16], image processing and image-model matching still demand for innovative ad-hoc solutions (especially when dealing with data collected in the space environment).

The image processing algorithm is designed to extract a set of 2D point features corresponding to salient parts of the target geometry. Specifically, an original combination of standard image processing tools is exploited. First, the Harris corner detector [17] is applied to the raw image, using a relatively-low intensity threshold (i.e., 0.01). Then, a subset of these corners is selected to ensure a uniform distribution on the region of the image plane occupied by the target (this aspect is particularly important for the image-model matching step). Clearly, the size of this subset (N_p) depends on the target-chaser distance, i.e., the farther the distance is, the lower becomes the number of points needed to adequately define the target appearance. At this point, the circular Hough Transform [18] is used to extract specific target components, such as appendixes, antennas, nozzles. Again, this information is useful to improve image-model matching performance. An example of application of this approach to the image of a scaled satellite mock-up, collected using an experimental facility available at Politecnico di Milano, is shown by Figure 3.
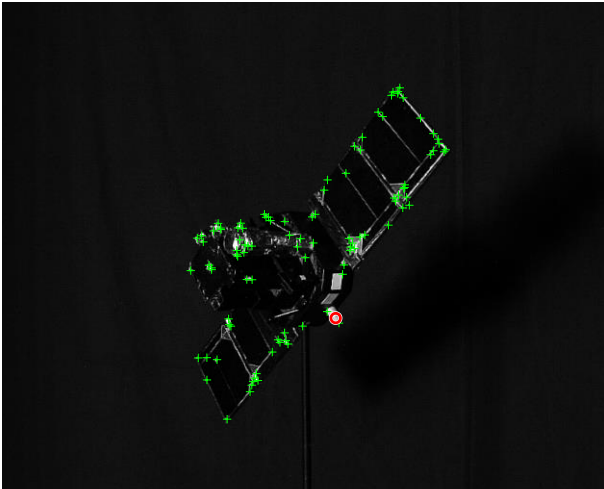

Figure 3. Example of implementation of the proposed approach for image processing. The output of the circular Hough Transform which allows extracting a specific appendix of the mock-up is highlighted by a red circle.

After image processing, image-model matching and pose parameters estimation are solved simultaneously. Specifically, a recursive, original approach based on the Random Sample Consensus (RANSAC) paradigm [15] is adopted for pose acquisition, while pose tracking is entrusted to the softPOSIT algorithm [19]. In this respect, it is worth outlining that two different PnP solvers are used. Indeed, the RANSAC-based approach developed for pose acquisition relies on the Efficient PnP (EPnP) algorithm [20], which provides a closed-form pose

solution, while softPOSIT is a non-linear solver. Both EPnP and softPOSIT exploit, as cost function, the reprojection error of the 3D landmark with respect to the corresponding 2D features (which is computed thanks to the classic equation of the perspective projection). However, while a fixed set of correspondences is used by the EPnP algorithm, softPOSIT optimizes the reprojection error by simultaneously updating the 2D-3D matches (which are represented by a purposely-defined assignment matrix).

With specific attention to the image-model association process, unlike standard RANSAC-based approaches which select randomly the initial consensus set, an original strategy is conceived in this work to accelerate algorithm's convergence while simultaneously reducing the risk of false image-model matches. Specifically, the Principal Component Analysis (PCA) [21], is used to classify the 2D features extracted by the image processing tool into multiple sub-sets based on their distribution on the image plane. This is done by analyzing eigenvectors and eigenvalues of the covariance matrix (Q) associated to the 2D pattern of corners. This covariance matrix can be computed using Eq. (X)

$$Q = \frac{1}{N_p} \begin{bmatrix} \sum_{i=1}^{N_p}(u_i - u_c)^2 & \sum_{i=1}^{N_p}(u_i - u_c)(v_i - v_c) \\ \sum_{i=1}^{N_p}(u_i - u_c)(v_i - v_c) & \sum_{i=1}^{N_p}(v_i - v_c)^2 \end{bmatrix} \quad (9)$$

where (u_i, v_i) and (u_c v_c) are the focal-plane coordinates of the ith extracted corner and image centroid, respectively. This classification allows carrying out the random association process considering smaller subsets of points. Indeed, also the 3D landmarks can be classified in different subsets. For instance, the landmarks belonging to the spacecraft solar arrays or antennas, are likely to be located far from the target centroid on the image plane and distributed in accordance to the principal directions of the 2D pattern of corner features. Finally, the image-model association is further aided exploiting the locations on the image plane of the target components detected using the circular Hough Transform.

4. HARDWARE DESIGN AND IMPLEMENTATION

This section provides an overview of the hardware design of VINAG. As shown in the schematic block diagram reported in Figure 4, VINAG is comprised of a Central Unit (VCU), the Camera System, including the Star tracker, and the IMU. As illustrated in Figure 5, the VCU includes all the electronic modules that can be grouped in one single and compact unit, so to minimize the impact on the volume and mass resources of the spacecraft. Two cameras for the vision-based navigation, the Star Tracker and the IMU are stand-alone units, to take into account the

specific accommodation requirements. In particular, two cameras for pose estimation are adopted, aiming at improving the reliability, by introducing a redundancy for that component which, as explained in the following, presents specific constraints in the selection of the image sensor. The schematic diagram reports the electrical interfaces between the different modules and units of VINAG and also the ones with the hosting spacecraft. A SpaceWire link, working up to 200Mbit/s and a redundant CAN bus are foreseen for the data exchange between VINAG and the GN&C, while for the input power I/F a 28V unregulated bus has been envisaged.
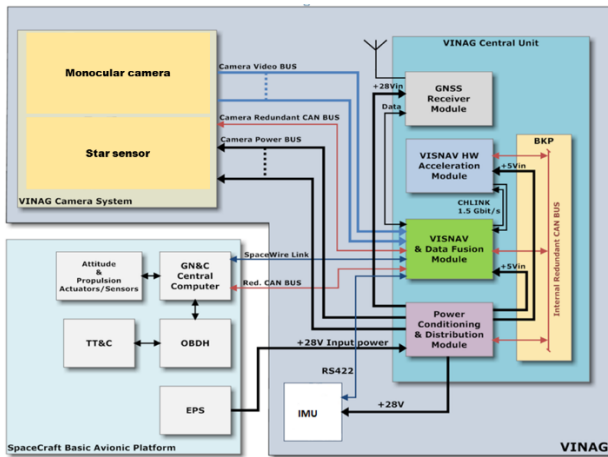
Figure 4. *VINAG Architecture and Interfaces.*
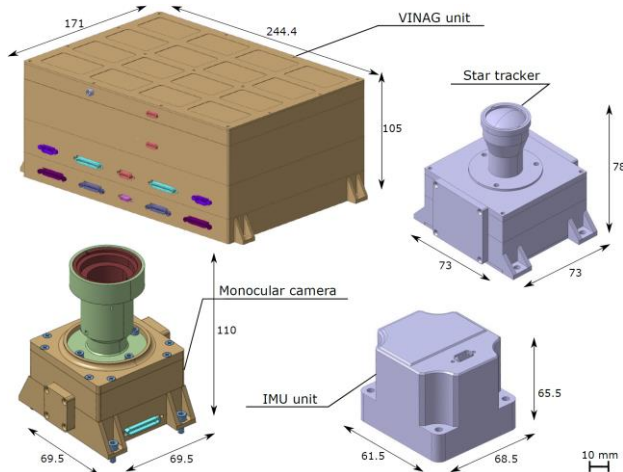
Figure 5 VINAG hardware CAD models.

4.1 VINAG Central Unit

Vision-based Navigation & Data Fusion and VISNAV HW acceleration modules

In the basic configuration the VCU is composed by the VISNAV (VISion-based NAVigation) & Data Fusion Module (VDFM), the VISNAV HW acceleration module, the GNSS Receiver Module, the Power Conditioning & Distribution Module (PCDM) and the Backplane Board

(BKP) that implement the power and data lines interconnection between all the modules.

The number and functionalities of the modules, the mechanical and electrical interfaces and all the architecture of the VCU have been defined with an high degree of modularity, so that it can be easily "customized and extended" to applications requiring a different grade of performances and redundancy, by adding further boards/modules and re-designing only the BKP of the system.

The VISion based Navigation (VISNAV) & Data Fusion Module (VDFM) is the core of VINAG Central Unit; it is based on a Microsemi RTG4 Flash FPGA and takes care of the video data acquisition from the Camera System, the image data processing and the monocular pose determination, the reception of the data coming from the GNSS receiver and the IMU and finally the implementation of the navigation data fusion algorithms. For the execution, at the required rate, of the VISNAV algorithms, representing the most demanding computational load, the VDFM can dispose (when needed) of an HW Acceleration Module that is based on two Xilinx Virtex XQR5VFX130 SRAM FPGAs.

The XQR5XVFX130 can be considered the first high performance rad-hard reconfigurable FPGA for processing-intensive space Systems. It is able to work at higher clock rate and provides embedded memory with higher capacity w.r.t. the RTG4 and therefore it is very effective when implementing complex image processing algorithms. It presents, as drawback, a higher power consumption, but, being used as accelerator, it is not always active or it is used at low duty cycles.

The RTG4 represents the Microsemi's fourth-generation flash-based FPGA offering above all, as advantage w.r.t. the Xilinx XQR5XVFX130, significant lower power consumption and a much better radiation hardness, The RTG4 provides also more logic resources (LUT and Flip Flops), that are very useful to cover the large set of functionalities. The lower power consumption (about a factor 5 w.r.t. the XQR5VFX130 SRAM FPGA) is very important for the power budget of the entire system because the VDFM is always powered on, since it takes care also of the overall control of the VINAG system and acts as supervisor of the functionalities of other components of the System, like RAM based FPGAs, camera system, GNSS, etc.

The RTG4 FPGA is immune to radiation (SEU) induced changes in configuration, due to the robustness of the flash cells used to connect and configure logic resources and routing tracks. No background scrubbing or reconfiguration of the FPGA is needed in order to mitigate changes in configuration due to radiation effects. Therefore the RTG4 FPGA is able to ensure nominal performances in the harshest radiation environments, such

Cold Start worst case TTFF	50.5 s	Warm Start worst case TTFF	9 s

as space flight LEO, MEO, GEO, HEO and deep space. This is a significant advantage w.r.t. the XQR5VFX130 for which the configuration memory is not immune to the radiation and the hardness is obtained by design, with a residual upset rate of five events per year in GEO.

The very large logical resources of the RTG4 are mainly dedicated to the HW implementation of the algorithms, or parts of them, requiring intensive-computing. In the same RTG4 FPGA is also implemented a SW IP core Processor that is employed for the control of the entire VINAG system and to run algorithms or only the high level of them, involving a computational load compatible with a SW implementation.

Bidirectional data transfer between the VDFM and the HW Acceleration Module is carried out at very high data rate (up to 1.575Gbit/s) by means of two Channel Link SerDes, working in opposite directions.

GNSS receiver

A spaceborne GNSS Receiver is under development for VINAG by Space Technology S.r.l. The receiver, multi-constellation can process the GALILEO E1 and GPS L1 C/A signals and it is based on a single ZynQ FPGA. To the best of the authors knowledge, it is the first European GNSS Receiver in single FPGA, or single ASIC form that integrates a Fast Acquisition Unit (FAU) and a GNSS Tracker, of up to six PRNs, in a single digital chip. The FAU and Tracking modules are used to estimate the Pseudo Range and the Doppler observables, input of the absolulte navigation filter, described in Section 3.1. The main characteristics of the GNSS Receiver, configured for a LEO mission, are summarized in Table 1.

Note that for GEO missions, the GNSS receiver of VINAG will adopt a different and space grade FPGA and will have a sensitivity equal or higher than 28 dB-Hz.

Table 1. Space Technology LEO GNSS Receiver characteristics and tested performances

GNSS Receiver Char.	Value	GNSS Receiver Char.	Value
Doppler Excursion	+/-60KHz	Doppler rates	+/-620Hz/s
Supported Constellation	GPS L1 C/A and GALILEO L1C/L1B	Number of Correlator Channels	>= 6
Acquisition Threshold @+/-60KHz	37dB-Hz	Acquisition Threshold @+/-40KHz	35dB-Hz
Acquisition time for GPS L1 C/A single PRN	40 ms	GALILEO L1 single PRN Acquisition time	95 ms

4.2 Cameras System

Monocular camera for pose estimation

The VINAG Camera System is composed by two CMOS Monocular cameras and one Star Tracker. The CMOS Monocular camera is a very compact, low power and high performance CMOS Camera, specifically designed, by TSD, for space applications on board small platforms.

Figure 6. VINAG Monocular Camera.

The electronics of the camera is based on an ACTEL FPGAs and adopts high-reliability components available with different qualification levels; the FPGA can be the ACTEL Flash-based RT3PE3000L or the Antifuse RTAX2000, the memory for temporary video image storage can be a 256Mbyte SDRAMs by 3D-plus or Aeroflex, the LVDS Serializer can be the DS90CR287MTD by National or the UT54LVDS217-UCC by Aeroflex, etc. The Focal Plane Assembly can be equipped with a 1024x1024[pixel], space grade image sensor, acquiring monochrome images up to 10[frame/s], or with an higher resolution 2048x2048[pixel] or 1920x1080(1080p)[pixel] COTS image sensor, acquiring color images, with a frame rate up to 60[frame/s]. The COTS sensors have been selected by TSD following a qualification campaign, including radiation tests too; however, in case of a COTS sensor is required (due to the specific optical requirements of the mission), two cameras (nominal and redundant) are foreseen, to take into account the reduced radiation tolerance offered by the sensor and consequently redundant camera I/Fs are foreseen on the VCU. The image acquisition can be synchronized with an external trigger or a self-generated internal one. The CMOS Monocular camera is provided with a CAN bus interface for the camera configuration & control and a Channel Link Serializer for the image data transmission to the VDFM at 1.2Gbit/s. The camera adopts a very rugged, conduction cooled, thermal- structural design and it is equipped with ±50° FOV lens. A more detailed description of this camera can be found in [22].

Star sensor

The Star sensor adopted in VINAG, is a compact, low power consumption (< 1W), low mass (< 1kg) device,

suitable for micro- and nano-satellites, characterized by an output rate of 5 Hz and a bore-sight accuracy of 2.5 arcsec and roll axis accuracy of 5 arcsec.

4.3 IMU

The Inertial Measurement Unit (IMU) for the VINAG system is a MEMS based equipment, with state-of-the-art bias stability on the order of 0.1deg/hr for gyroscopes and 0.015mg for accelerometers.

Low cost and highly compact HW platform version

For less demanding missions in term of duration, reliability and rad-tolerance, with consequent lower economical budgets, it has been foreseen the development of a low cost and higher compact version of the VINAG HW platform, suitable also to the application on smaller platform (including Cubesat). For that alternative version it is foreseen the substitution of some of the currently adopted space grade electronic components, strongly impacting on the costs and the size of the modules, with COTS devices. The RTG4, the XQR5VFX130 and the memory chips will be substituted with the Microsemi SMART Fusion 2, the Xilinx Kintex or Zynq and COTS memory chips, carefully selected and submitted to a qualification test campaign. The selected COTS devices are able of withstanding, and also with a significant margin, the Total Ionizing Dose (TID) levels expected by the target mission for this alternative low cost version; mitigation actions (EDAC, memory scrubbing, latch-up detection and protection, etc.) are on the contrary foreseen against the single-event effects, for which those components exhibit not enough immunity levels. For the power devices like DC/DC converters, switching and linear voltage regulators, transceivers and for the passive components it will be adopted the same qualification space grade adopted for the VINAG hi-rel version. The smaller size and the lower power consumption of the new set of components will allow the merging of the HW acceleration module into the VFDM, the reduction of the PCDM dimensions and a consequent and significant reduction of the VCU volume, mass and power.

5. HW/SW PARTITIONING

The goal of the hardware/software (HW/SW) partitioning was dividing the computational load into two parts: one that executes sequentially, on a microprocessor (the "software instruction driven processor") and another part, that runs on the FPGA (the "hardware parallel processor"), in such a way to minimize power, size, and cost and maximize the performance, thus allowing real time operations.

As first step, we analyzed the control flow and data flow within the navigation architecture and determined what are the computationally expensive parts, which are better implemented in hardware. With a software profiling, the time complexity of each function and sub-function were measured. Figure 7 and Figure 8 illustrate the main computation steps respectively in absolute navigation and in relative navigation. While Figure 9 and Figure 10 report the corresponding relative execution time.

The HW/SW partitioning of VINAG is essentially based on the computational complexity of the algorithms but also on the characteristics of the adopted FPGAs. As mentioned in Section 4, VINAG adopts two different set of FPGA devices, depending on the mission type (one for low cost LEO missions and one for longer GEO missions with higher radiation tolerance). Therefore, for each FPGA set a different HW/SW partitioning is required.
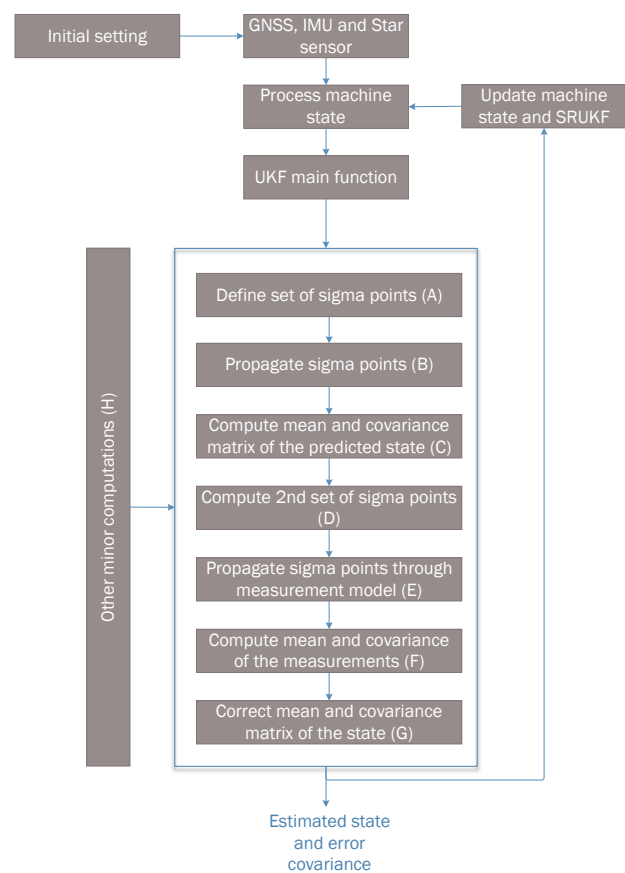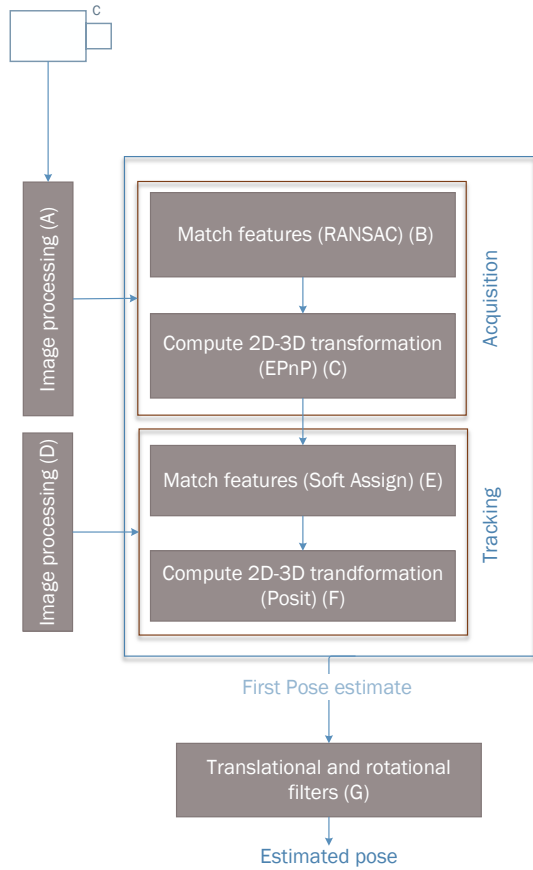

Figure 7. Absolute navigation computation steps.

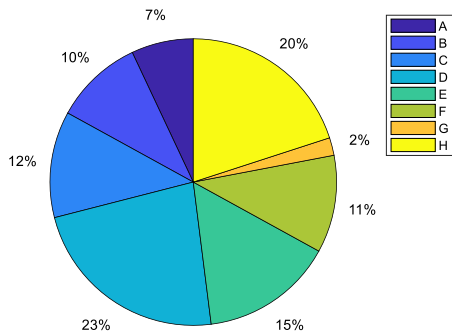*Figure 8. Pose determination computation steps.*

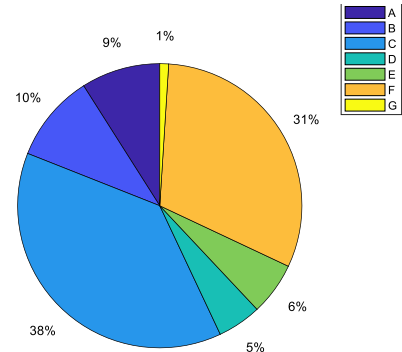*Figure 9. Execution time of each computation step illustrated in Figure 7.*

Figure 10. Execution time of each computation step illustrated in Figure 8.

6. SIMULATED PERFORMANCE

6.1 Models and assumptions

GNSS observations

A constellation of 30 GPS and 30 Galileo satellites was assumed for the simulation. GPS L1 and Galileo E1 signal power levels at the receiver position, were modelled realistically taking into account their 3D receiver and transmitters' antenna pattern.

A receiver sensitivity of 35 dB-Hz was assumed in LEO, while of 28 dB-Hz in GEO. Pseudoranges and pseudorange rates were modelled considering all the main source of error, also as function of the receiver characteristics and of the carrier-to-noise-ratio C/N_0.

Inertial Measurement Unit and Star sensor

IMU and Star sensor observations were modelled according to their characteristics summarized in Section 4. In particular, the IMU model includes linear and non-linear effects like scale factor, cross-coupling, saturation, quantization as well as a detailed noise model of angle (for the gyros) and velocity (for the accelerometers) random walk, bias instability and rate random walk [22].

Monocular camera

Due to the challenges of realistically reproducing in a software environment the imaging process of a monocular camera operating in space, performance assessment of the image processing tool is not included in the numerical simulations presented in this work. However, ad-hoc experimental tests are currently under development, whose results will be presented in future works. Based on this consideration, the operation of the monocular camera is simulated by projecting the 3D landmarks composing the simplified model of the target on the image plane. The error sources associated to the feature detection process are modeled as a Gaussian noise applied to the ideal landmark projection on the image plane. The standard deviation of this noise (σ_{pix}) is expressed in terms of a

certain number of pixel. According to recent results in the open literature [23], realistic values of σ_{pix} can range between 1 and 3 pixels. In addition to this random noise, the presence of a limited number of outliers, i.e., corners not corresponding to 3D landmarks in the model, is also considered.

6.2 Simulations results

Absolute navigation

The absolute navigation performance was preliminary evaluated by means of simulations in a LEO and GEO scenario. Simulation scenarios were defined using a high fidelity simulation tool developed by PoliMi, including non-uniform mass distribution of the Earth, solar radiation pressure, atmospheric drag, third body perturbation (sun and moon), gravity gradient and magnetic field perturbation. The PoliMi high fidelity astrodynamic tool has been developed to support the Mission Analysis and Design for different financed studies such as PlAtiNO and CHRISTMAS (ASI supported) and S3Net (H2020 framework study). Precisely, in LEO as reference, we assumed the THAS-I Nimbus platform characterized by a class cubic shape, size of [0.8, 0.8, 1.6] m, drag coefficient equal to 2.2 degrees and mass of 100 kg. The Keplerian orbital parameters of the reference initial orbit are: semi-major axis of 7158 km, eccentricity null, inclination of 98,5 degrees. In GEO we investigate the VINAG system capabilities in an orbit well above the GNSS constellations. The reference platform is the THAS-I PRIMA. In this case the Keplerian orbital parameters are: pericenter height of 36000 km, eccentricity and inclination both null. The data generated by the high fidelity simulation tool fed the sensor simulators (i.e IMU, GNSS receiver and Star sensor) according to the above defined models. Furthermore, simulations were carried out also including 300ms and 6μs/s of respectively receiver clock's bias and drift with the respect to satellites clock.

Figure 11 and Figure 12 display respectively the positioning and attitude determination errors in the considered LEO scenario. Similarly, Figure 13 and Figure 14 show the same errors in GEO scenario. In LEO, the positioning error has a standard deviation lower than 3 m on all the axes, while in GEO smaller than 6 m on x- and y- axes, and smaller than 1 m on z- axis. A poorer accuracy in GEO is expected by accounting for the Geometric Dilution Of Precision (GDOP) and also for an higher receiver noise due to lower signal power levels. The attitude estimation is always quite accurate with an error smaller than 0.06°in LEO and in GEO.

Furthermore, Figure 15 and Figure 16 show the number of total satellites effectively used with respect to the visible ones as result of the masking algorithm described above. As expected in GEO the average availability is lower than in LEO. The estimation accuracy obtained demonstrates

however the effectiveness of VINAG absolute navigation algorithm, in different scenarios (LEO and GEO).

VINAG Absolute Navigation Algorithm was successfully tested also in a laboratory Real-Time simulation environment. The algorithm developed in Matlab/Simulink® was processed in order to rapidly implement a real-time executable code by using the xPCTarget® tool with its automatic code generation features. The real-time test rig includes two machines: one dedicated to the sensor measurement generation and simulation data storage and the second one completely dedicated to navigation algorithm execution. The measurements were generated and transmitted (by using a point-to-point ethernet link), at the respective rate according to the sensor models described in the previous paragraphs.

The Absolute Navigation Algorithm machine is based on an Intel® Pentium® 4 processor at 3.00Ghz with 1Gb of RAM. In order to evaluate the worst case execution time a single task application was developed without any kind of code and execution optimization. Precisely, the real-time software is executed at a single base rate time of 0.01s.

The real-time simulation results shown a worst case Task Execution Time (TET) that depends on the availability of the measurements. Precisely, in absence of Star Sensor and GNSS receiver valid measurements the TET is evaluated around 1.89ms, while in presence of 26 satellites and Star Sensor measurement the computation takes about 3.48ms. This is due to the different dimensions of the state-output covariance matrix and related state correction computing. The average TET is however about 1.91ms taking into account the measurement timing and related computing load.

The simulated scenario in real-time is the same LEO scenario already described. Figure 17 and Figure 18 show a substantial replication of the numerical offline results already discussed assessing the correct implementation.

The Real-Time test results demonstrated the VINAG Absolute Navigation algorithm implementation feasibility in a Real-Time environment also providing an estimation of TET.
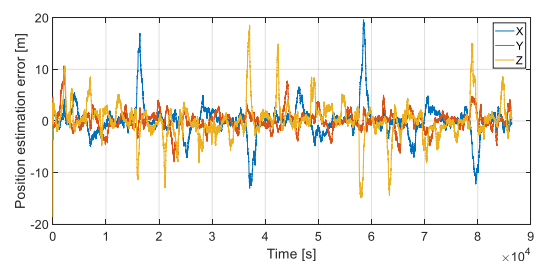

Figure 11. Position estimation error in the considered LEO trajectory.
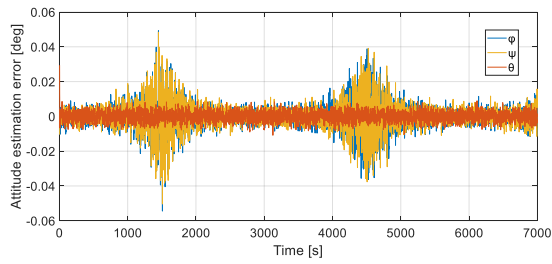
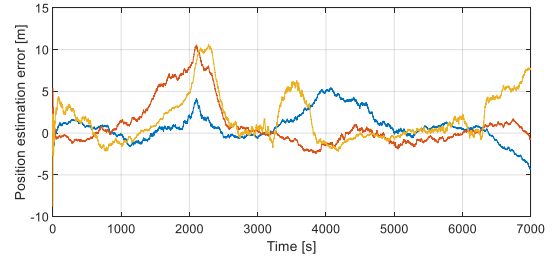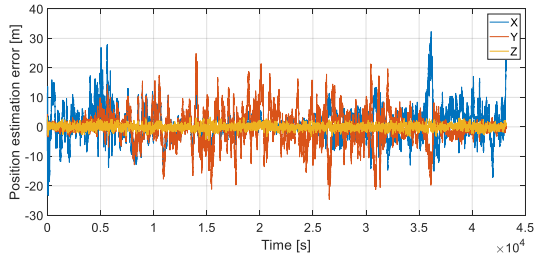*Figure 12. Attitude estimation error in the considered LEO trajectory.*

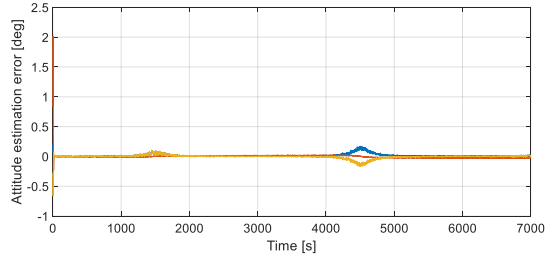*Figure 13. Position estimation error in the considered GEO trajectory.*

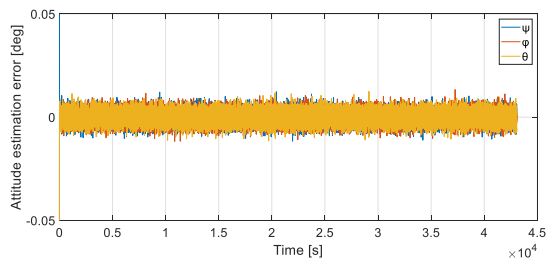*Figure 14. Attitude estimation error in the considered GEO trajectory.*

Figure 15. Number of GNSS satellites (or observations) used in the estimation in the considered LEO trajectory.

Figure 16. Number of GNSS satellites (or observations) used in the estimation in the considered GEO trajectory.

Figure 17. Position estimation error in the considered LEO trajectory.

Figure 18. Attitude estimation error in the considered LEO trajectory.

Relative navigation

For what concern the relative navigation, two different targets are tested: the ESA X-ray space observatory, XMM-Newton, representative of a large space debris, and one of the satellites of the Hispasat family, representing the next generation of SmallGEO platforms for telecommunication. The simplified models of the two targets are shown in Figure 19.
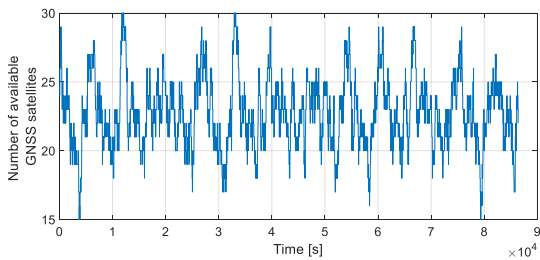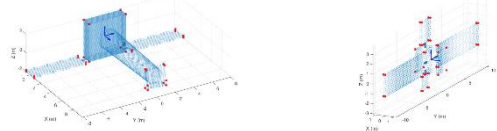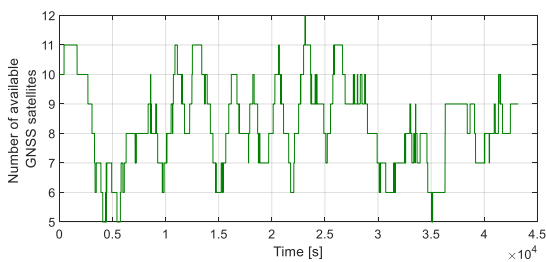

Figure 19. Targets simplified models. XMM (left) and Hispasat (right).

The LEO scenario is selected to test the relative navigation algorithm for the XMM case. On the contrary, the GEO reference orbit is used in the case of the Hispasat target. The assumed initial relative conditions are $\rho_{0-LEO} = [0, 30, 0]\ m$ and $\rho_{0-GEO} = [0, 40, 0]\ m$ for the position and $\dot{\rho}_0 = [0, -1, 0] * 10^{-4}\ m/s$ for the relative velocity in both cases, expressed in the local-vertical, local-horizontal (LVLH) reference frame fixed to the chaser spacecraft center of mass. The relative dynamics is simulated assuming a torque-free motion for the target spacecraft. Classical Euler equation for rigid body are used, by imposing the following initial conditions, equal in the two scenarios: $\omega_T = [0.1, 0, 0] deg/s$. To preliminary assess the performance of the proposed approaches for monocular pose determination, simulated noisy images of the target are generated. In particular, a value of $\sigma_{pix} = 1$ is considered. Moreover, a number of false corners

($n_{out} = 1$) is randomly located in the region of the image plane occupied by the target (according to a uniform distribution) to simulate the presence of outliers in the measurements provided by the image processing. A frequency of 1Hz is assumed for both pose determination and filtering block.

The estimation errors are defined as follows: $e_\rho = \sqrt{(x_i - \hat{x}_i)^2 + (y_i - \hat{y}_i)^2 + (z_i - \hat{z}_i)^2}$ is the position error where $\hat{x}_i$, $\hat{y}_i$, $\hat{z}_i$ are the position components estimates and x_i, y_i, z_i are the true position components, obtained by integrating the complete nonlinear differential equations of the unperturbed relative motion. The relative attitude error is computed as $e_R = \text{acos}\left(1 - \frac{\text{tr}(I - R_i^T \hat{R}_i)}{2}\right)$, with $\hat{R}_i$ being the estimated rotation matrix at time i. Figure 20 and Figure 21 report the relative position and attitude errors for both cases for a single run. The resulting performance are promising, in fact, the errors statistics for the presented cases are $\mu_{e_{\rho-LEO}} = 0.035\,m$ and $\mu_{e_{\rho-GEO}} = 0.02\,m$, $\sigma_{e_{\rho-LEO}} = 0.012\,m$ and $\sigma_{e_{\rho-GEO}} = 0.013\,m$ for the relative position and $\mu_{e_{R-LEO}} = 0.43\,deg$ and $\mu_{e_{R-GEO}} = 0.46\,deg$, $\sigma_{e_{R-LEO}} = 0.246\,deg$ and $\sigma_{e_{R-GEO}} = 0.218\,deg$ for relative attitude.
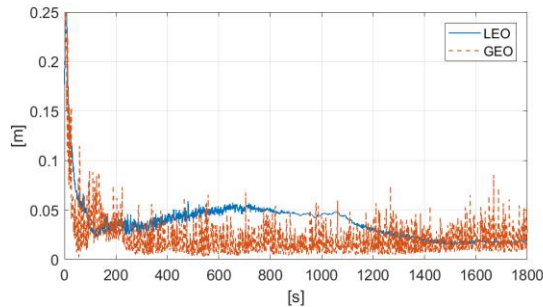

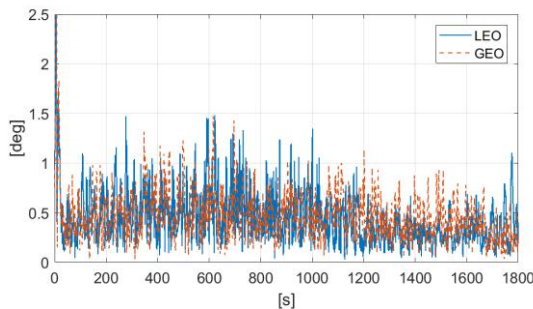*Figure 20. Relative Position Error.*

Figure 21. Relative Attitude Error.

7. CONCLUSIONS

In this paper, we presented the system VINAG, currently under development by a team of Italian companies and universities, co-financed by the Italian Space Agency. VINAG has been specifically designed for on-board, real-time absolute and relative spacecraft navigation. More specifically, orbit and attitude determination is ensured by integrating in a SRUKF architecture a GNSS receiver, an IMU and a Star sensor. While, a monocular camera is used for vision-based pose estimation of uncooperative orbiting targets. We described the architecture, the navigation algorithms, the HW design and the HW/SW partitioning and finally we reported carried out numerical simulations of the navigation performance. In the next step of the project, the capabilities of VINAG will be also validated through hardware-in-the-loop simulations and testing.

8. REFERENCES

[1] V. Capuano, G. Cuciniello, V. Pesce, R. Opromolla, S. Sarno, M. Lavagna, M. Grassi, F. Corraro, G. Capuano, P. Tabacco, F. Meta, M. L. Battagliere and A. Tuozzi, "VINAG: A HIGHLY INTEGRATED SYSTEM FOR AUTONOMOUS ON-BOARD ABSOLUTE AND RELATIVE SPACECRAFT NAVIGATION," in *The 4S Symposium*, 2018.

[2] E. W. R. Van Der Merwe, The Square-Root Unscented Kalman Filter for State and Parameter-Estimation, vol. 6, IEEE International Conference on Acoustics, Speech, and Signal Processing, 2001. Proceedings. (ICASSP '01), 2001, pp. 3461 - 3464.

[3] M. Madden, Gravity Modeling for Variable Fidelity Environments, Keystone, CO: AIAA Modeling and Simulation Technologies Conference and Exhibit, 2006.

[4] G. E. Montenbruck O., Satellite Orbits Models, Methods and Applications, Springer Verlag, 2000.

[5] F. L. Markley, Attitude Error Representations for Kalman Filtering, Vols. 26, N.2, AIAA - Journal of Guidance, Control, and Dynamics, 2003, pp. 311-317.

[6] M. Andrle and J. L. Crassidis, "Geometric Integration of Quaternions," *Journal of Guidance, Control, and Dynamics,* vol. 36, no. 6, pp. 1762-1767, 2013.

[7] L. Chang, B. Hu and G. Chang, "Modified Unscented Quaternion Estimator Based on Quaternion Averaging," *Journal of Guidance, Control, and Dynamics ,* vol. 37, no. 1, pp. 305-309, 2014.

[8] R. Zanetti, G. Holt, R. Gay, C. D'Souza, J. Sud, H. Mamich, M. Begley, E. King and C. F. D., "Absolute Navigation Performance of the Orion Exploration Flight Test 1," *Jounral of Guidance,*

Control, and Dynamics, vol. 40, no. 5, pp. 1106-1116, 2017.

[9] V. Pesce, M. Lavagna and R. Bevilacqua , "Stereovision-based pose and inertia estimation of unknown and uncooperative," *Advances in Space Research,* pp. 236-251, 2017.

[10] D. Simon, Optimal state estimation: Kalman, H infinity, and nonlinear approaches, John Wiley & Sons, 2006.

[11] K. Yamanaka and F. Ankersen, "New state transition matrix for relative motion on an arbitrary elliptical orbit," *Journal of guidance, control, and dynamics,* pp. 60-66, 2002.

[12] M. Zamani, J. Trumpf and R. Mahony, "Nonlinear attitude filtering: a comparison study," *arXiv:1502.03990,* 2015.

[13] A. Saccon, J. Trumpf, R. Mahony and A. P. Aguilar, "Second-order-optimal minimum-energy filters on lie groups," *IEEE Transactions on Automatic Control,* pp. 2906-2919, 2016.

[14] M. Lourakis and X. Zabulis, "Model-Based Pose Estimation for Rigid Objects," in *International Conference on Computer Vision Systems*, St. Petersburg, 2013.

[15] M. A. Fischler and R. C. Bolles, "Random sample consensus: A Paradigm for Model Fitting with Applications to Image Analysis and Automated Cartography," *Communications of the ACM,* pp. 381-395, 1981.

[16] S. Sharma and S. D'Amico, "Comparative assessment of techniques for initial pose estimation using monocular vision," *Acta Astronautica,* pp. 435-445, 2016.

[17] C. Harris and M. Stephens, "A combined corner and edge detector," in *Alvey vision conference*, 1988.

[18] H. K. Yuen, J. Princen, J. Illingworth and J. Kittler, "Comparative study of Hough Transform methods for circle finding," *Image and Vision Computing,* pp. 71-77, 1990.

[19] D. Philip, D. DeMenthon, R. Duraiswami and H. Samet, "SoftPOSIT: Simultaneous pose and correspondence determination," *International Journal of Computer Vision,* p. 259–284, 2004.

[20] V. Lepetit, F. Moreno-Noguer and P. Fua, "Epnp: An accurate o (n) solution to the pnp problem," *International Journal of Computer Vision,* p. 155–166, 2009.

[21] S. Wold, K. Esbensen and P. Geladi, "Principal component analysis," *Chemometrics and intelligent laboratory systems,* pp. 37-52, 1987.

[22] G. Capuano, R. Ascolese, D. Titomanlio, P. Longobardi, M. De Nino and G. Formicola, "A Multi-Ocular Smart System for Vision-based Space Navigation," in *65th IAC International Astronautical Congress*, Toronto, Canada, 2014.

[23] S. Sharma, J. Ventura and S. D'Amico, "Robust Model-Based Monocular Pose Initialization for Noncooperative Spacecraft," *Journal of Spacecraft and Rockets,* 2018.